Electronic Supplementary Material (ESI) for Nanoscale Horizons.

Supplementary Information

Realizing the Extraction of Carbon from WC to in Situ Formation of W/WC Heterostructures with Efficient Photoelectrochemical Hydrogen Evolution

*Zongkui Kou, Tingting Wang, Zonghua Pu, Lin Wu, Kai Xi, Shichun Mu**

This file includes:

S1. Experimental methods

Structural characterization. Scan electron microscopy images were performed on a JEOL S4800 scan electron microscopy operated at 15 kV. Field emission transmission electron microscopy (TEM) and high resolution TEM (HRTEM) images were carried out on a JEM 2100F transmission electron microscope operated at 200 kV. High-angle aberration-corrected dark-field scan transmission electron microscopy (HAADF-STEM)-energy-dispersive X-ray spectroscopy (EDS) with spherical aberration correction were taken on a JEM 1011 transmission electron microscope operated at 300 kV. The samples were prepared by dropping ethanol dispersion of the samples onto ultrathin carbon film-coated copper TEM grids (Beijing Zhongjingkeyi Technology Co., Ltd) using pipettes and dried under ambient condition. X-ray photoelectron spectroscopy (XPS) tests were done with VG Scientific ESCALAB 210 electron spectrometer. Powder X-ray diffraction (PXRD) patterns were collected on a Rigaku diffractometer using a Cu-Kα X-ray source operated at 45 kV and 100 mA, at a rate of 2 °/min from 5 to 80°. Raman spectroscopy was analyzed using a RENISHAW Raman microscope with a Ne-He laser excitation operated at 633 nm wavelength.

Computational details. DFT calculations were performed using the plane-wave technique implemented in the Cambridge Sequential Total Energy Package. The ion-electron interaction was treated within the projector-augmented plane wave pseudopotentials [1, 2]. The generalized gradient approximation expressed by Perdew-Burke-Ernzerhof functional and a plane-wave cutoff energy of 420 eV were used in all computations [3]. The electronic structure calculations were employed with a Fermi-level smearing of 0.1 eV for all surface calculations and 0.01 eV for all gas-phase species. The Brillouin zone was sampled with $6 \times 6 \times 1$ k-points. The convergence of energy and forces were set to 1×10^{-5} eV and 0.02 eV/Å, respectively. The WC

(0001) planes were constructed with eight atomic layers where the top two layers and adsorbate were allowed to fully relax. For all W cover surfaces, monolayered or bilayered W (110) planes was used to substitute for top layers of WC and a vacuum region of around 15 Å was set along the z direction to avoid the interaction between periodic images (Figure S6) [4]. The Pt (111) surface was modeled with four atomic layers where only the top layer and adsorbate were allowed to fully relax [5].

ΔG_H for all surfaces can be described as: $\Delta G_H=\Delta E_H+\Delta E_{ZPE}-T\Delta S$, where ΔE_H, ΔE_{ZPE}, T and ΔS respectively represents the hydrogen adsorption energy, the zero point energy difference, the system temperature (298.15 K, in this work), the entropy difference between the adsorbed state and the gas phase. For all system, ΔE_H can be calculated by subtracting individual energy from DFT total energies. Moreover, to eliminate the effect of hydrogen coverage on ΔE_H, the monolayer hydrogen (ML_H) adsorption coverage is given to all computations (**Figure S6**). E_{ZPE} was computed by summing vibrational frequencies over all normal modes ($E_{ZPE}=1/2\sum\hbar\nu$).

Fabrication of photocathode and PEC measurements. Si nanowire arrays were fabricated via the method described in the literature [6]. Subsequently, 40 μl of the above ink was uniformly spin-coated onto a 15 mm*15 mm Si nanowire electrode at 500 rpm and dried at 2500 rpm. Ohmic contact to the backside of electrode was made by scratching with Ga-In eutectic and affixing a Cu wire to it. PEC experiments were performed in a custom-built circular photochemical cell with a circular ~0.4 cm^2 aperture, which was sealed by the working electrode. Light was provided by a PL-XQ500 W Xe arc lamp from Beijing Precise Technology Co., Ltd. Its power density was adjusted to 100 mW cm^{-2} and calibrated with an optical power meter equipped with a thermopile detector. LSV curves were collected at scan rate of 10 mV s^{-1}.

Electrochemical measurements. To prepare the catalyst ink, 5 mg of active materials and 10 μl of Nafion solution (5 wt%) were dispersed in a mixture of 90 μl of H_2O and 900 μl of ethanol (v/v, 1/10) with the assistance of ultrasonication for at least 1 h. Then 40 μl of the ink was dropcast onto a glassy carbon electrode of 5 mm in diameter (catalyst loading 1 mg cm^{-2}). Electrochemical measurements were performed in a standard three-electrode set-up in 0.5 M H_2SO_4 solution, using a saturated calomel electrode (SCE), the catalyst loaded glassy carbon electrode, and a graphite rod as the reference, working and counter electrode, respectively. Linear sweep voltammetry (LSV) was carried out at a scan rate of 5 mV s^{-1}. Electrochemical impedance measurements were carried out at 200 mV of overpotential in the frequency range of 100,000-0.1 Hz. I-t chronoamperometric response was conducted in H_2 saturated 0.5 M H_2SO_4 solution at η=200 mV for 10, 000 s.

S2. Digital photos of by-products

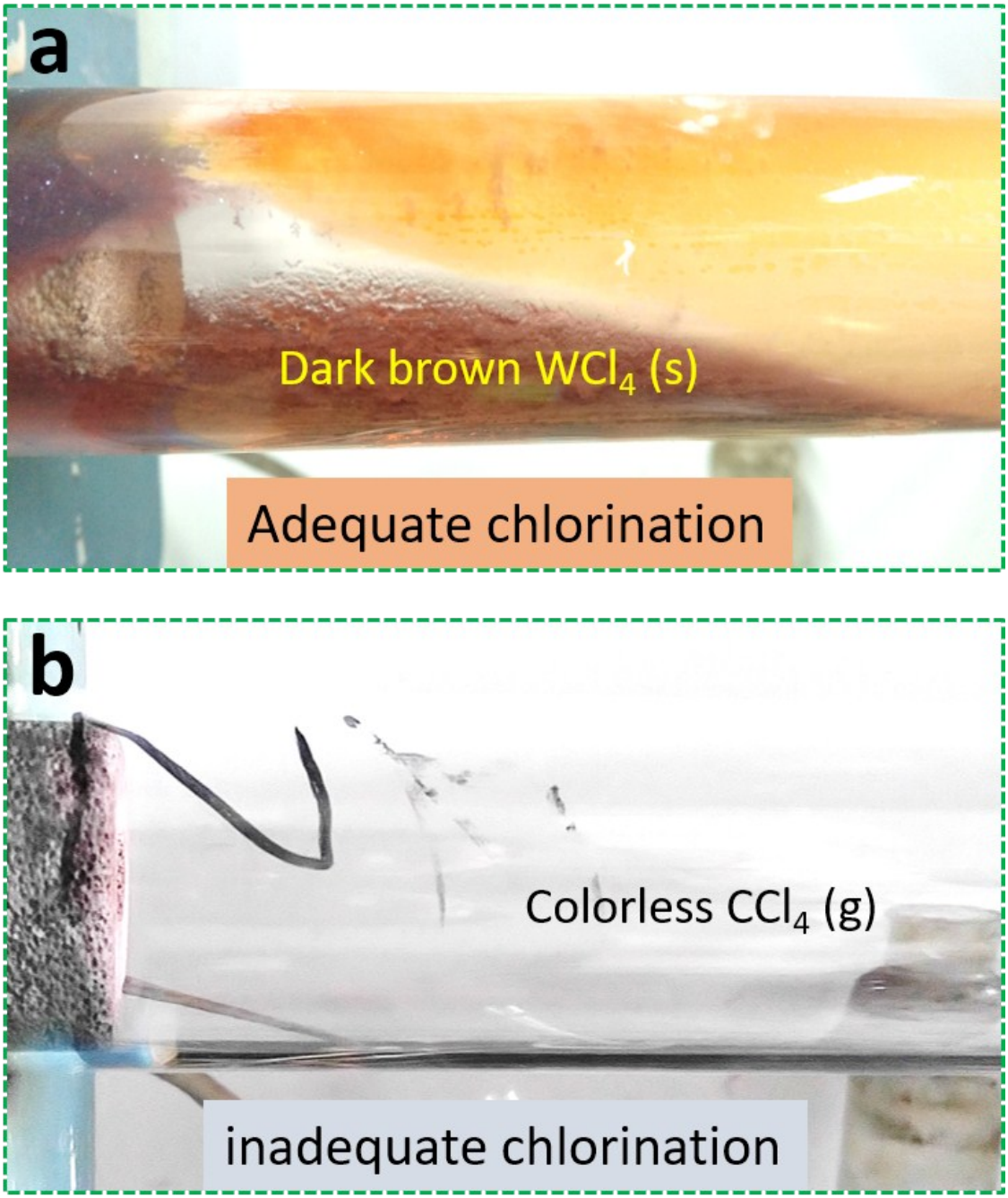

Figure S1. Digital photos of two different by-products: (a) dark brown tungsten tetrachloride and (b) colorless carbon tetrachloride. When adequate chlorine gas (χ=2.6) was introduced into reaction setup, gaseous tungsten tetrachloride escaped from the setup and desublimated when it cools down outside the reaction region. However, the introduction of inadequate chlorine gas (χ=1.3) leads to emission of colorless carbon tetrachloride.

S3. Morphology and structure of the WC

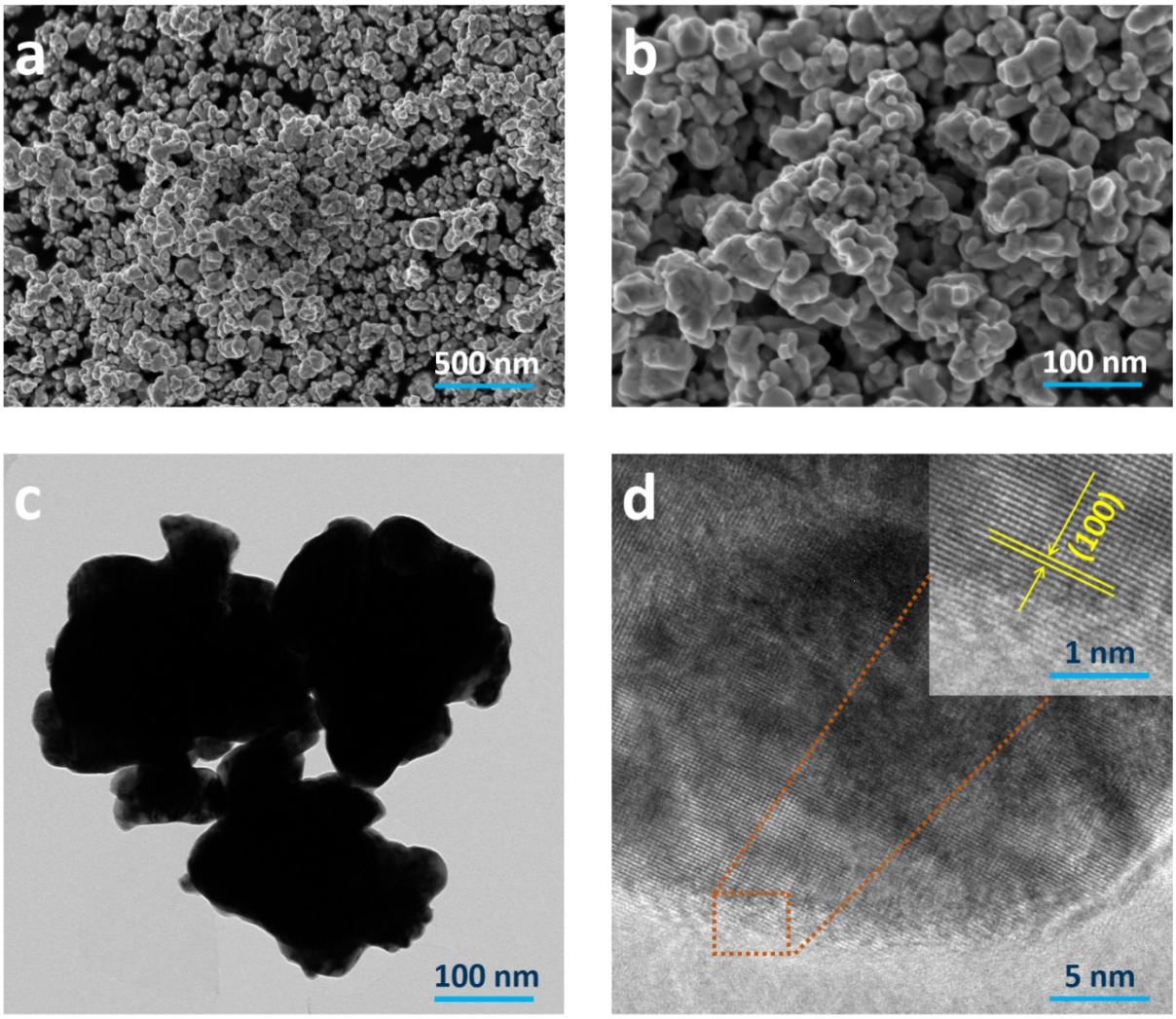

Figure S2. (a, b) SEM images with different resolutions of the pristine WC. (c, d) TEM and HRTEM images of the pristine WC. The inset image in d presents a WC (100) surface with interplanar spacing of 2.53 Å.

S4. Morphology and surface information of the W/WC heterostructure

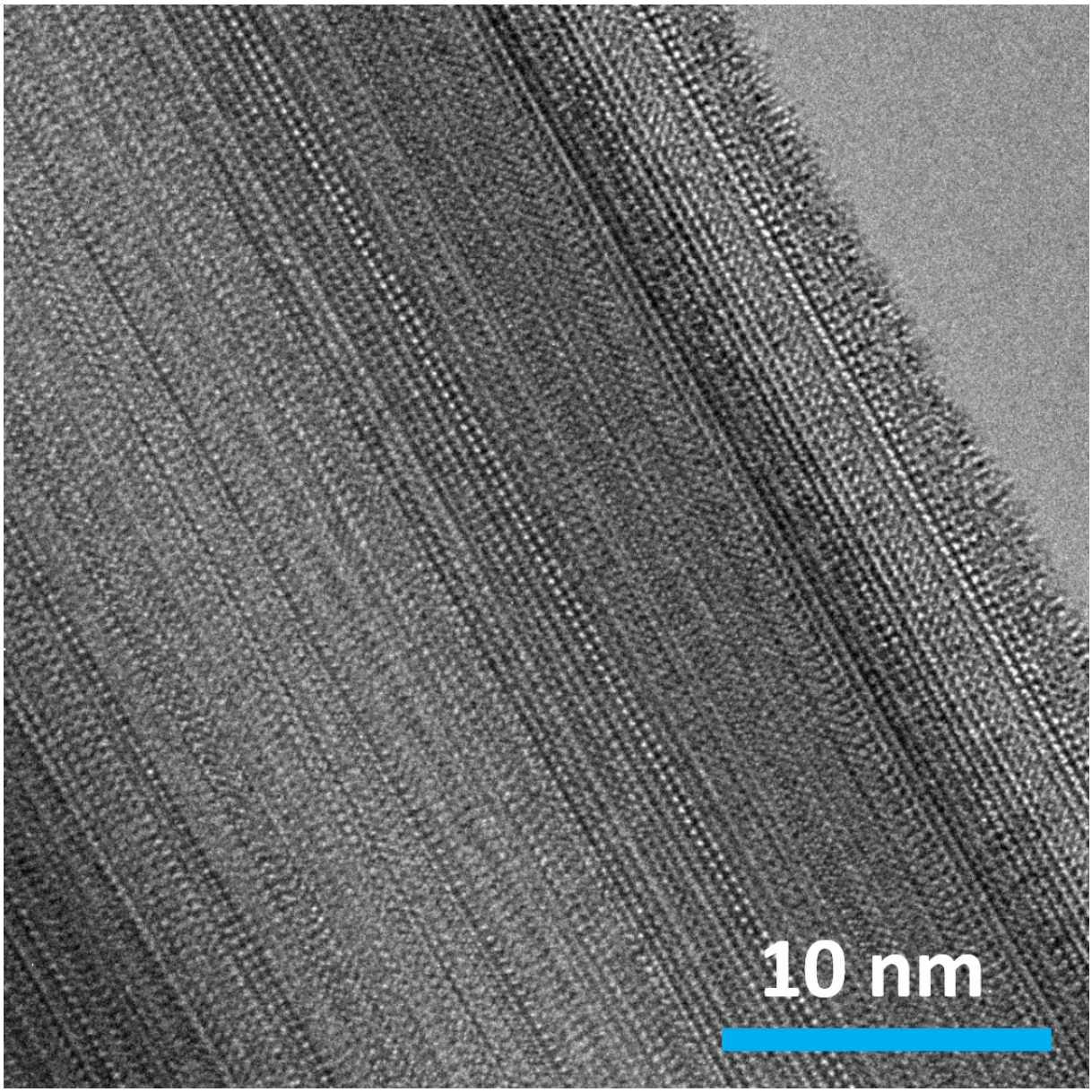

Figure S3. HRTEM image of a surface of the produced W/WC which is used to simulate 3D surface plot (Figure 1e).

S5. Morphology and structure of the Sintering WC

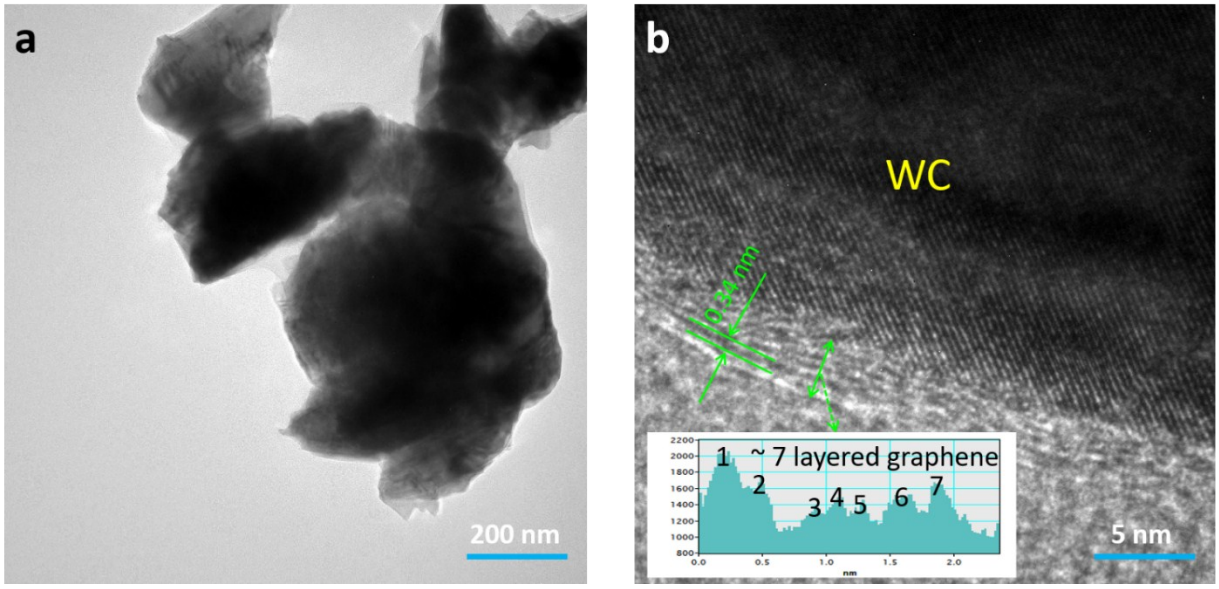

Figure S4. Sintering WC produced by the chlorination method under conditions of 1000 ℃, χ=0 and 4 h for holding time. (a) TEM image and (b) HRTEM image. The inset image discloses seven layers of graphene on WC due to surface segregation of carbon atoms when suffering from high temperature. Moreover, the TEM image presents the attachment of WC by surface sintering.

S6. The influence of thermodynamic configurations on the composition and microstructure of the final products

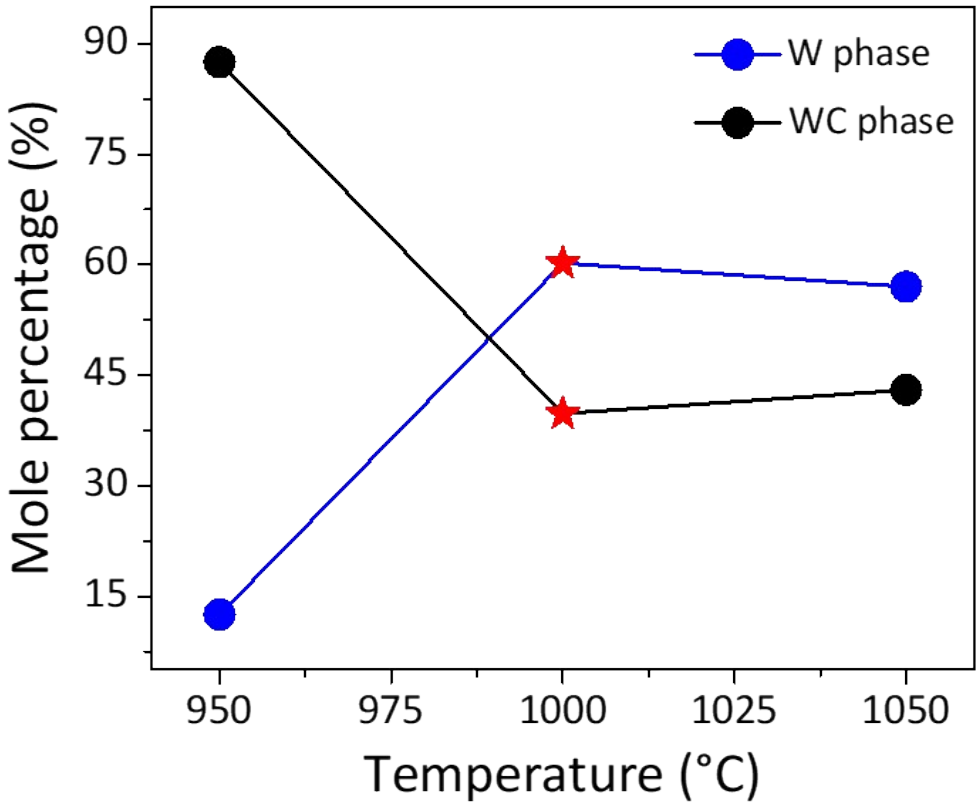

Figure S5. The influence of reaction temperature on the composition of the final products: Calculated contents of the W and WC phases based on PXRD patterns (Figure 3a).

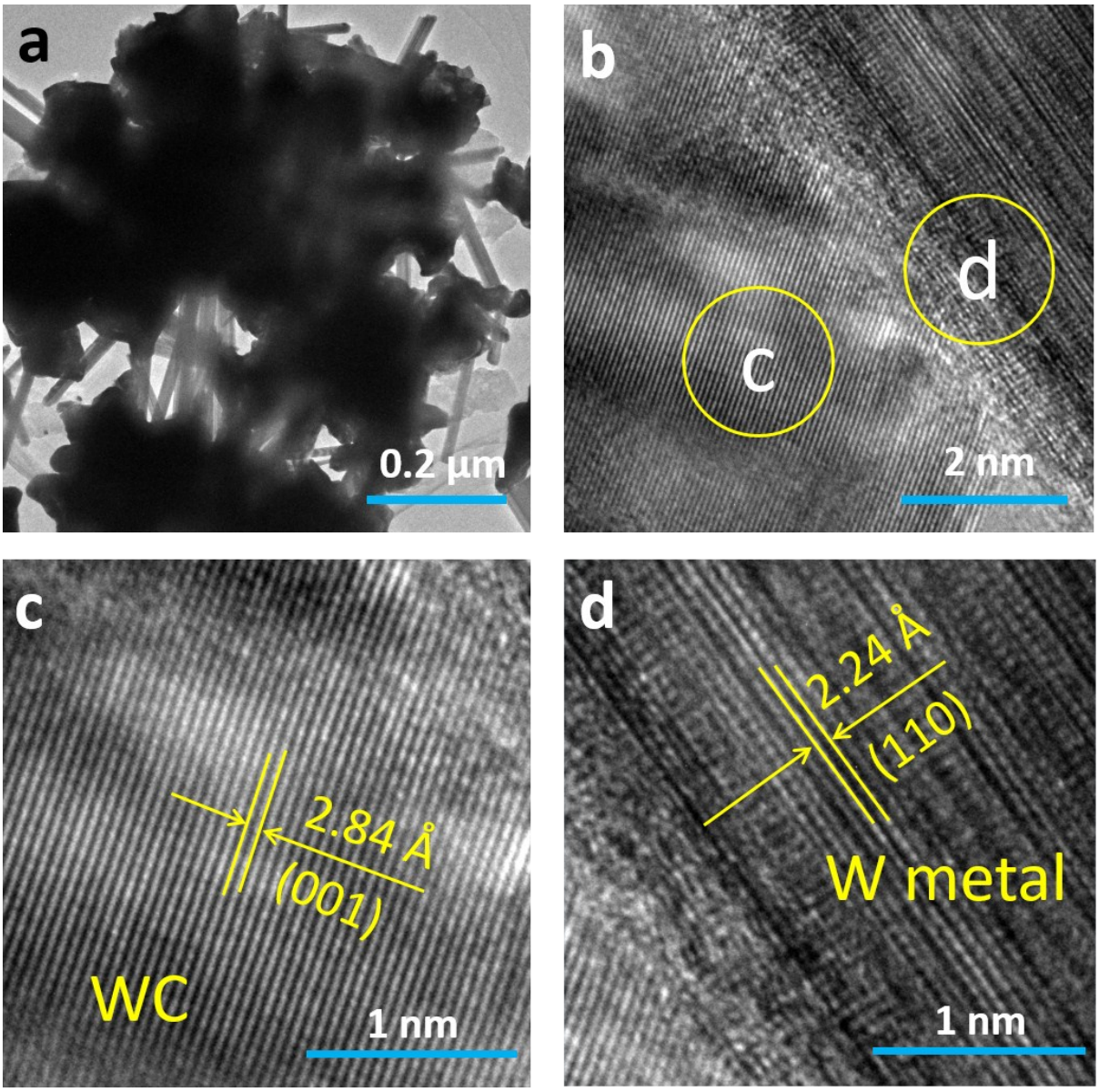

Figure S6. WC-W/WC composite produced by the second step at 950 ℃. (a) TEM image, (b) HRTEM image, (c) atomic lattice of (001) facet on WC and (d) atomic lattice of (110) facet on W cover layers.

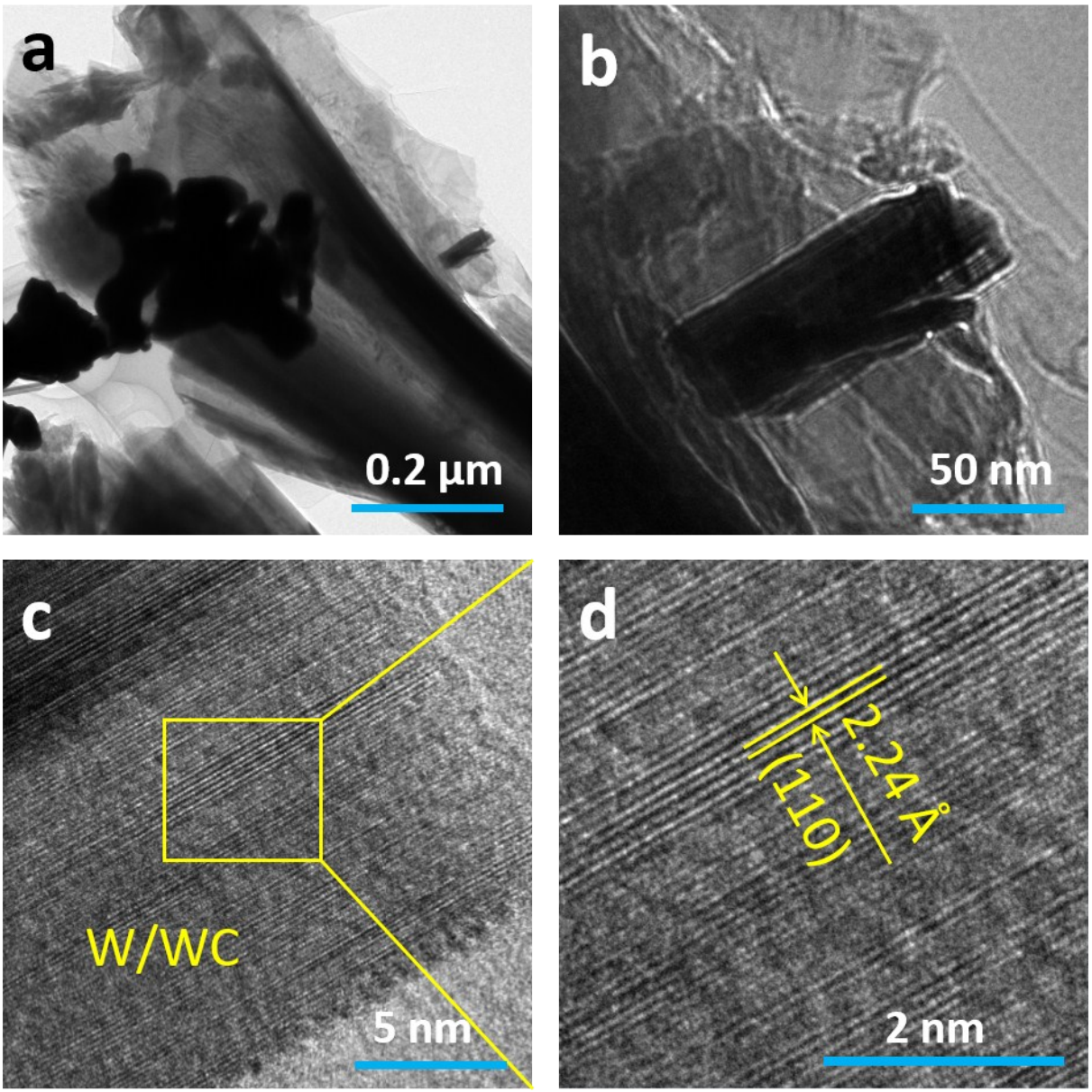

Figure S7. Broken W/WC produced by the second step at 1050 ℃. (a, b) TEM images, (c) HRTEM image, (d) atomic lattice of (110) facet on W cover layers. TEM image presents a gradual fracture of nanoribbon microstructure at the temperature of high to 1050 ℃.

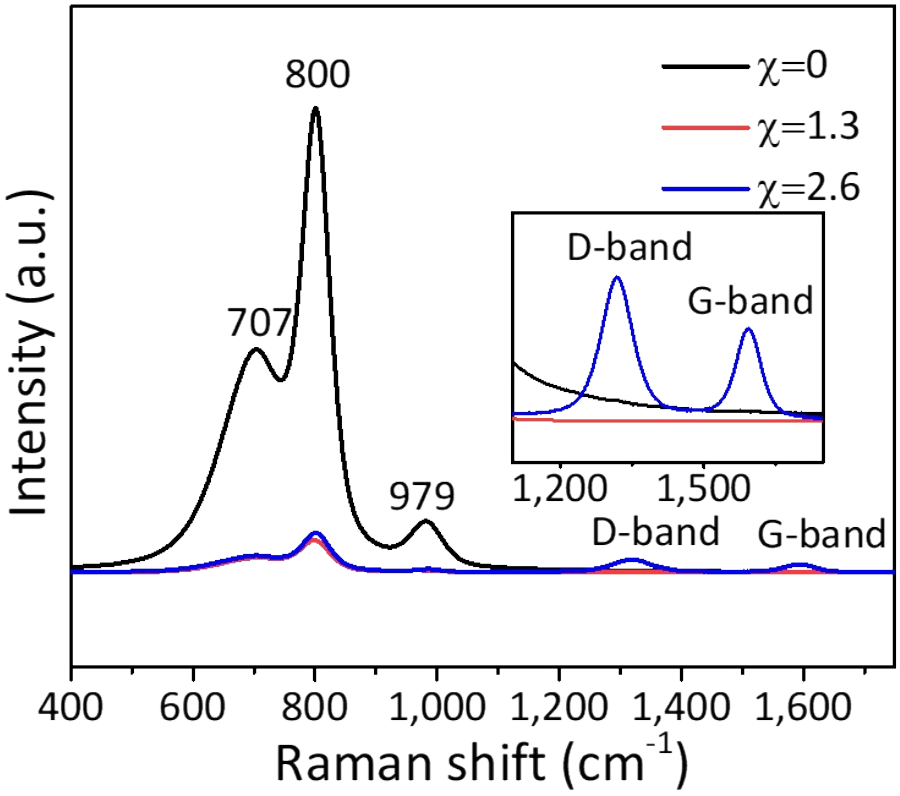

Figure S8. The influence of different χ on the composition of the final products: Raman spectra of the final products.

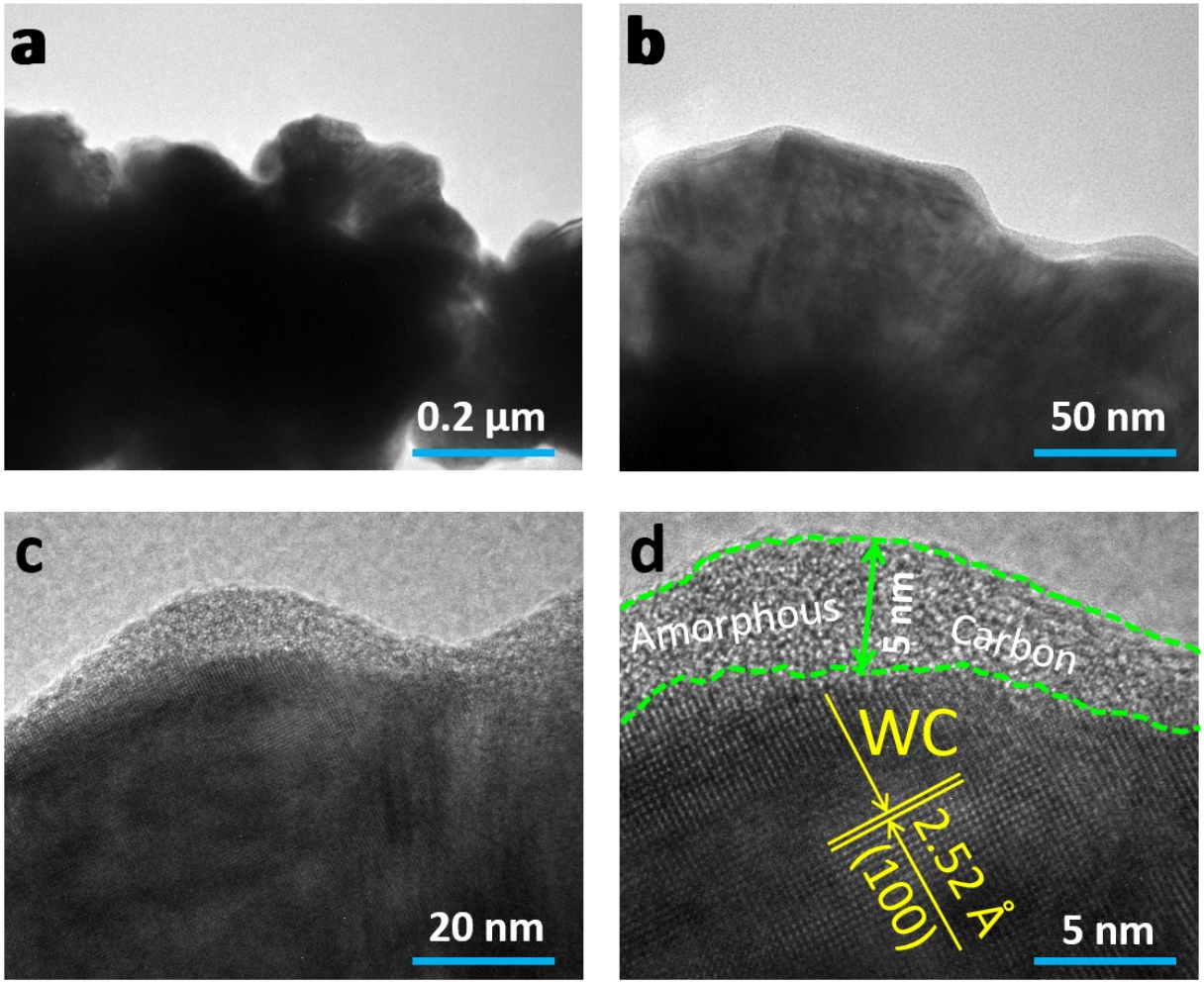

Figure S9. WC@CDC produced by the first step at 1000 ℃ and χ=2.6. (a, b) TEM images, (c) HRTEM image, (d) atomic lattice of (100) facet and amorphous carbon layer on WC. It is obvious that bigger χ results in step one reaction. As a result, amorphous carbon coated WC can be obtained.

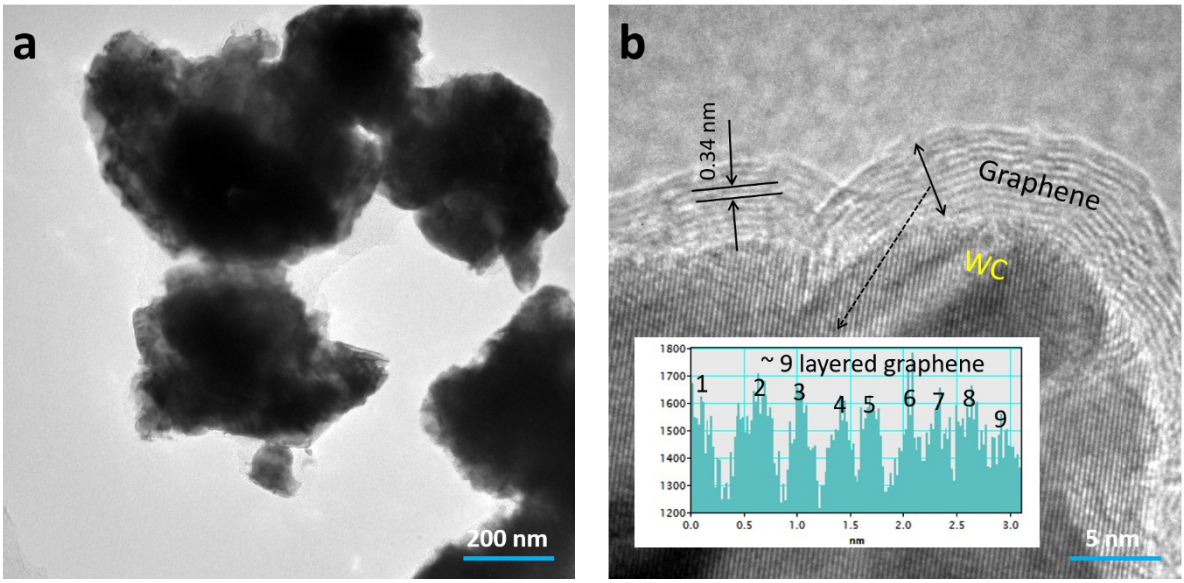

Figure S10. WC coated by nine layered graphene (WC@NLG) produced at 1000 ℃ for longer holding time of 8 hours. (a) TEM image and (b) HRTEM image. The inset image in c discloses nine layers of graphene on WC. Moreover, the TEM image presents the attachment of WC by surface sintering.

S7. Geometric structure and d-band center of the as-studied systems.

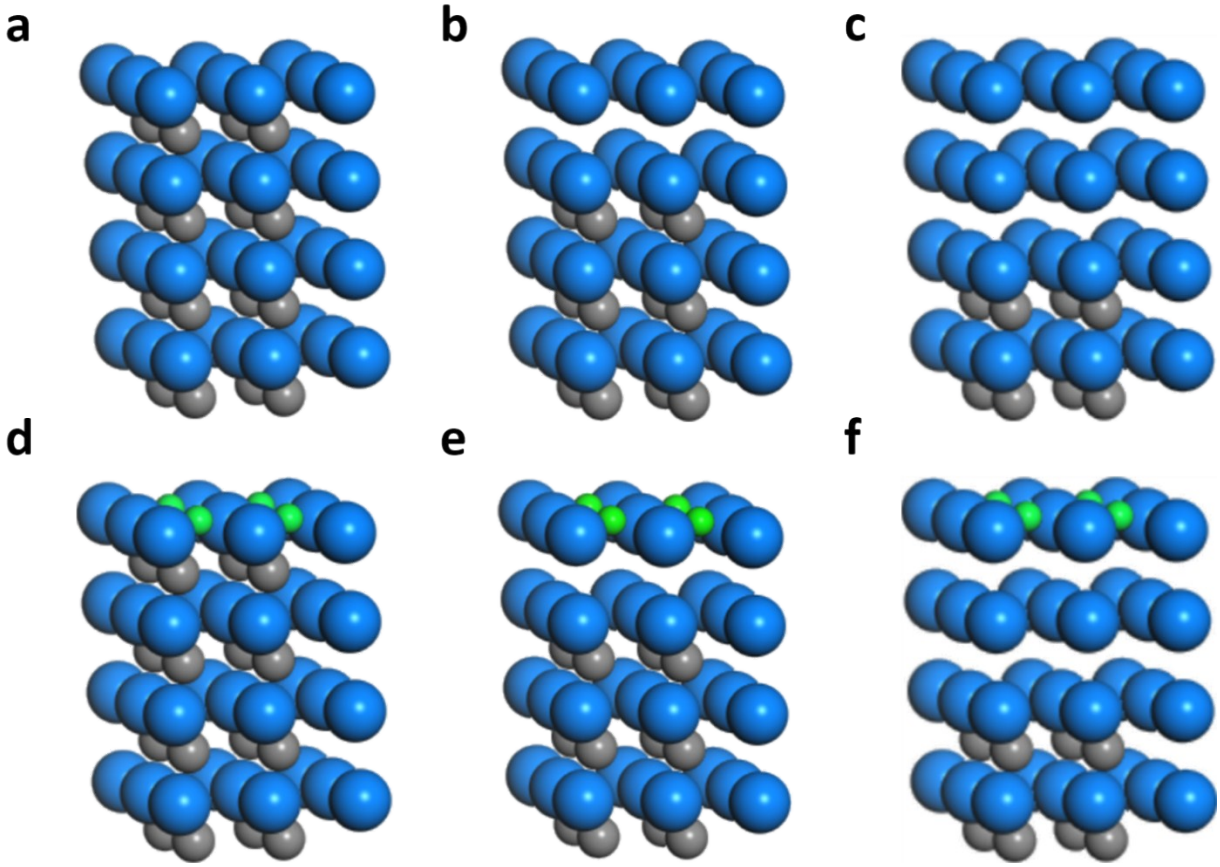

Figure S11. Geometric structure of (a) WC (0001), (b) 1LW/WC, (c) 2LW/WC, (d) $1ML_H$ on WC (0001), (e) $1ML_H$ on 1LW/WC and (f) $1ML_H$ on 2LW/WC in side view.

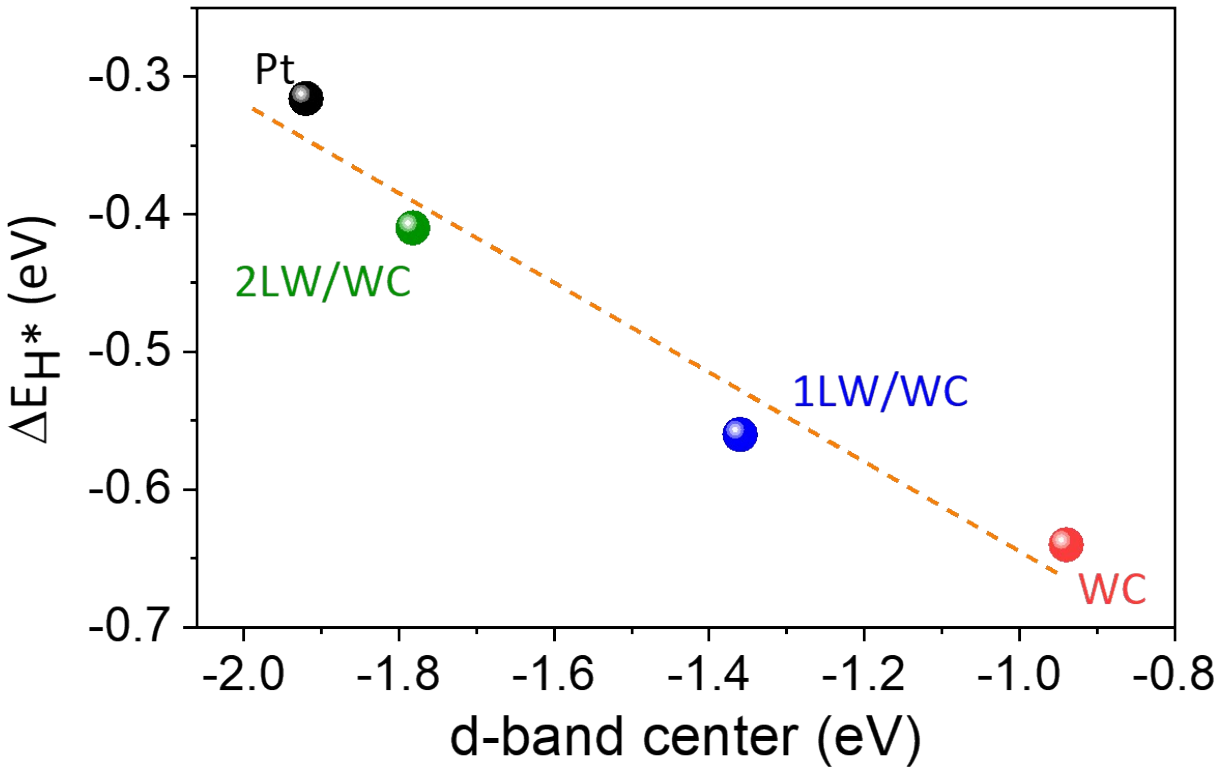

Figure S12. Correlation of hydrogen adsorption energy (ΔE_H) at a layer of hydrogen absorption coverage with the d-band center over various studied systems.

S8. The morphology of the W/WC integrated on the p-type Si nanowires.

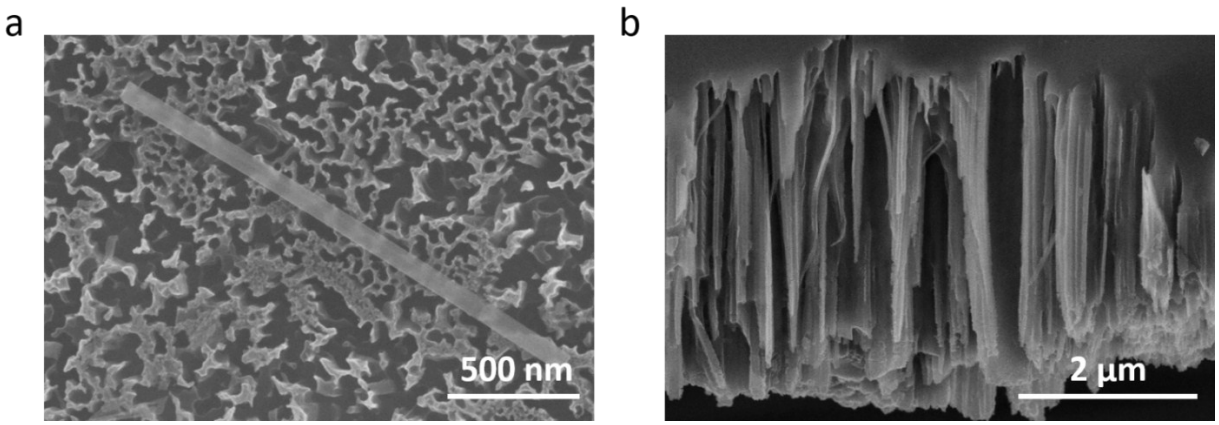

Figure S13. SEM images of the photocathode loaded with W/WC.

S9. The morphology, composition and surface information of the W/WC before and after the HER experiment.

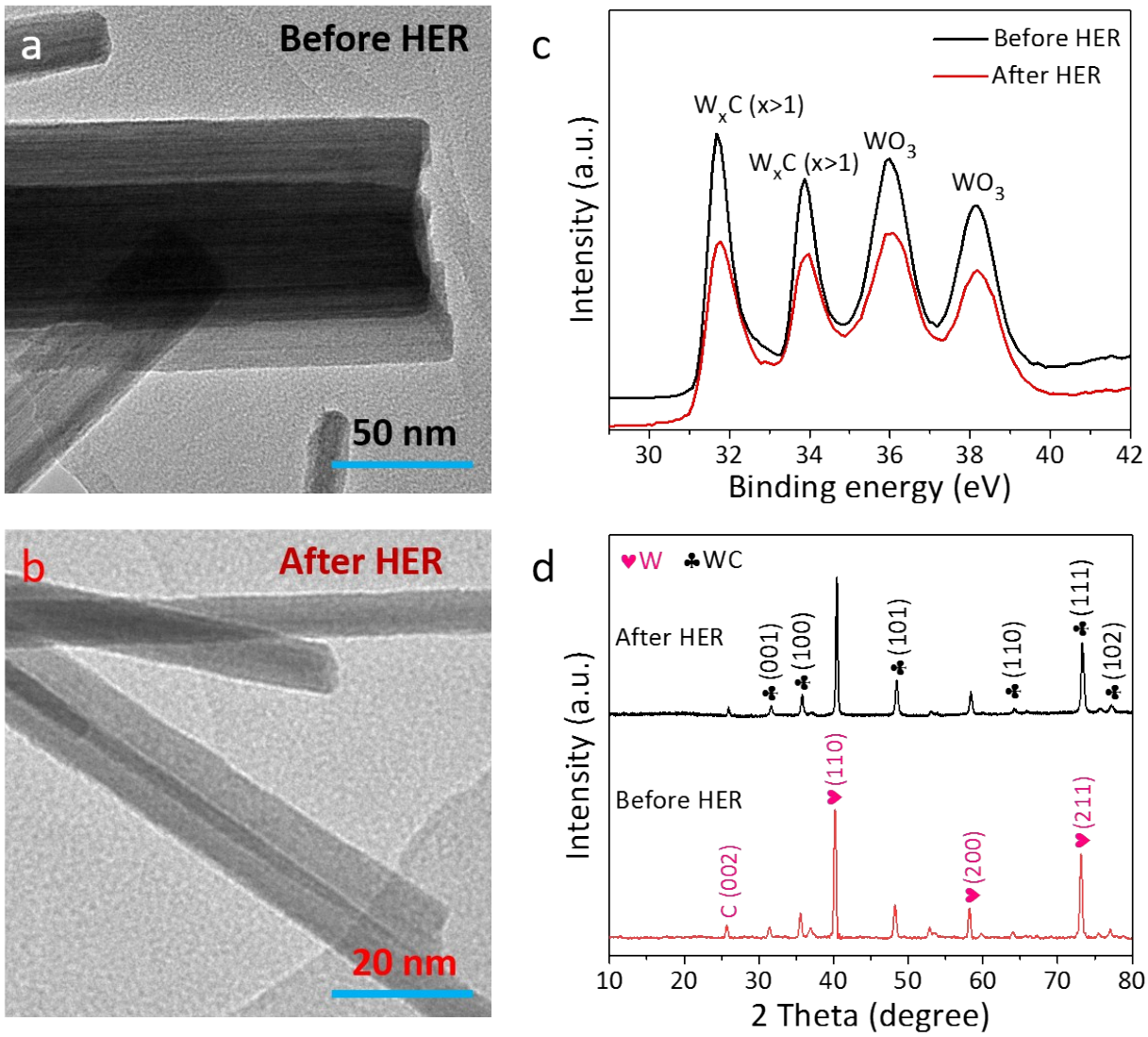

Figure S14. (a, b) TEM images, (c) XRD patterns and (d) W 4f XPS spectra of W/WC before and after the HER experiment. To prepare samples for the durability studies, catalyst powder was loaded onto p-type Si NWs to achieve a high loading of 1 mg cm^{-2}, and subjected to continuous 120 min current-time response measurement at 0.1 V vs RHE. Then, catalyst powder was sonicated off the electrode and dried in a vacuum oven at 120 ℃ to remove the solvent. Repeating five times ensure sufficient catalyst amount for subsequent TEM, XRD and XPS studies.

S10. The influence of thermodynamic configurations on the HER activities of the final products

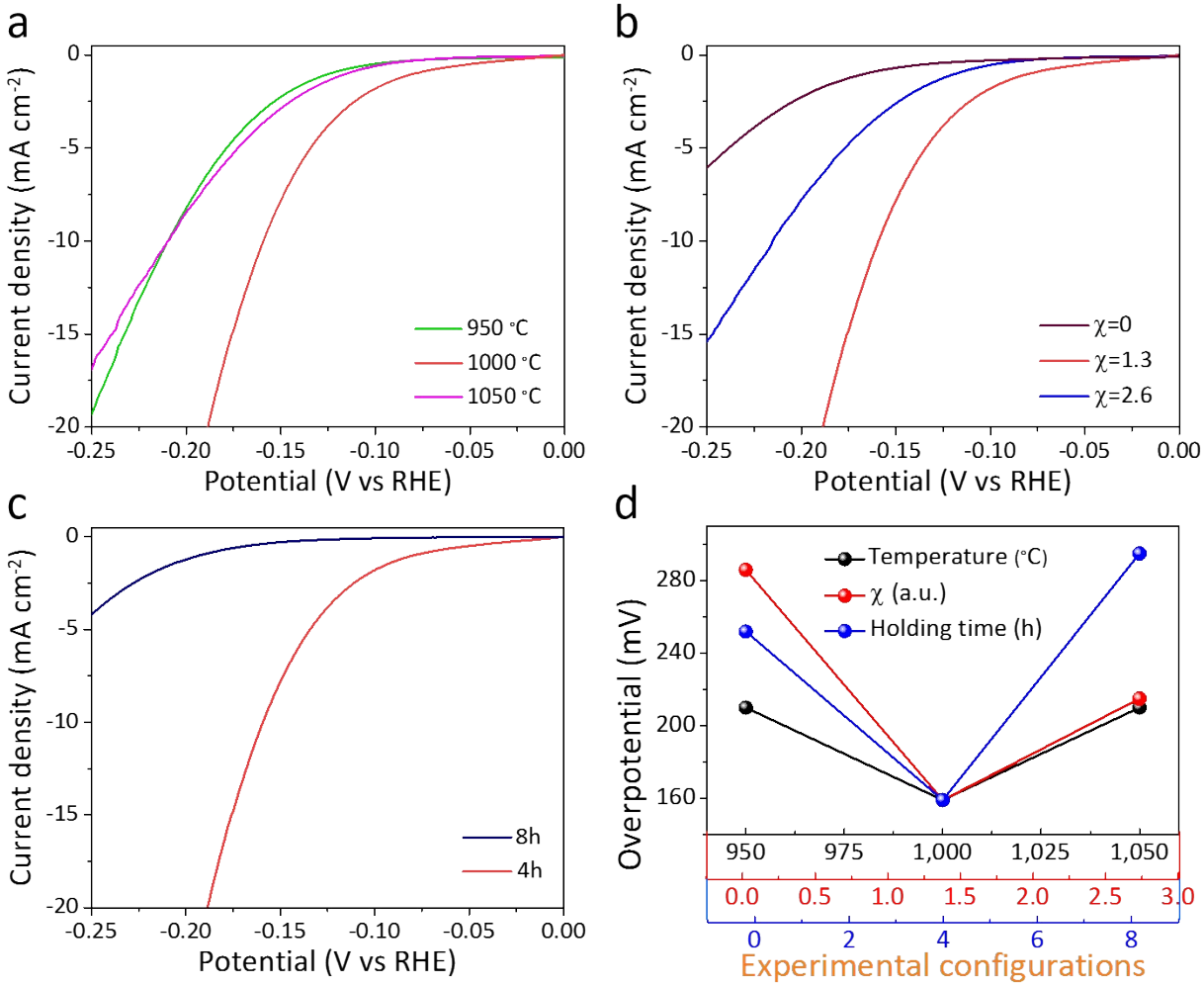

Figure S15. The influence of various experimental configurations on the HER activity of the final products. (a-c) The HER polarization curve of the products at different temperature (a), χ (b) and holding time (c). (d) Comparison of overpotentials at a current density of 10 mA cm^{-2}. Obviously, 1000 ℃, χ=1.3 and 4 h for holding time can obtain the highest HER performance.

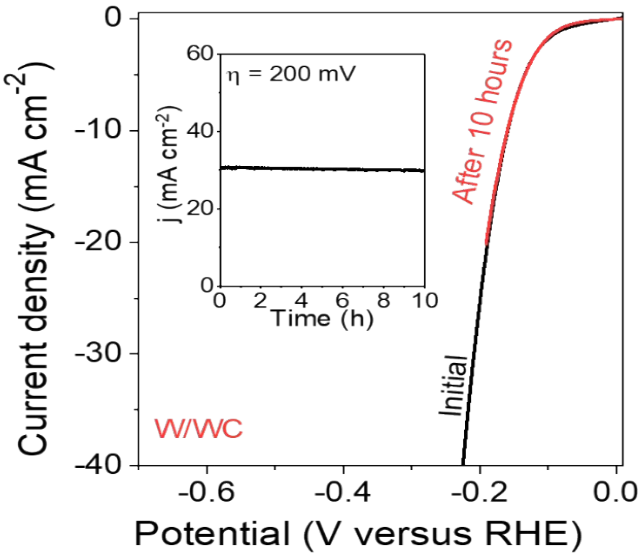

Figure S16. Polarization curve of W/WC heterostructures before and after i-t chronoamperometric response (the inset image) at η =200 mV for 10 hours.

S11. The mechanism on enhancing HER activity

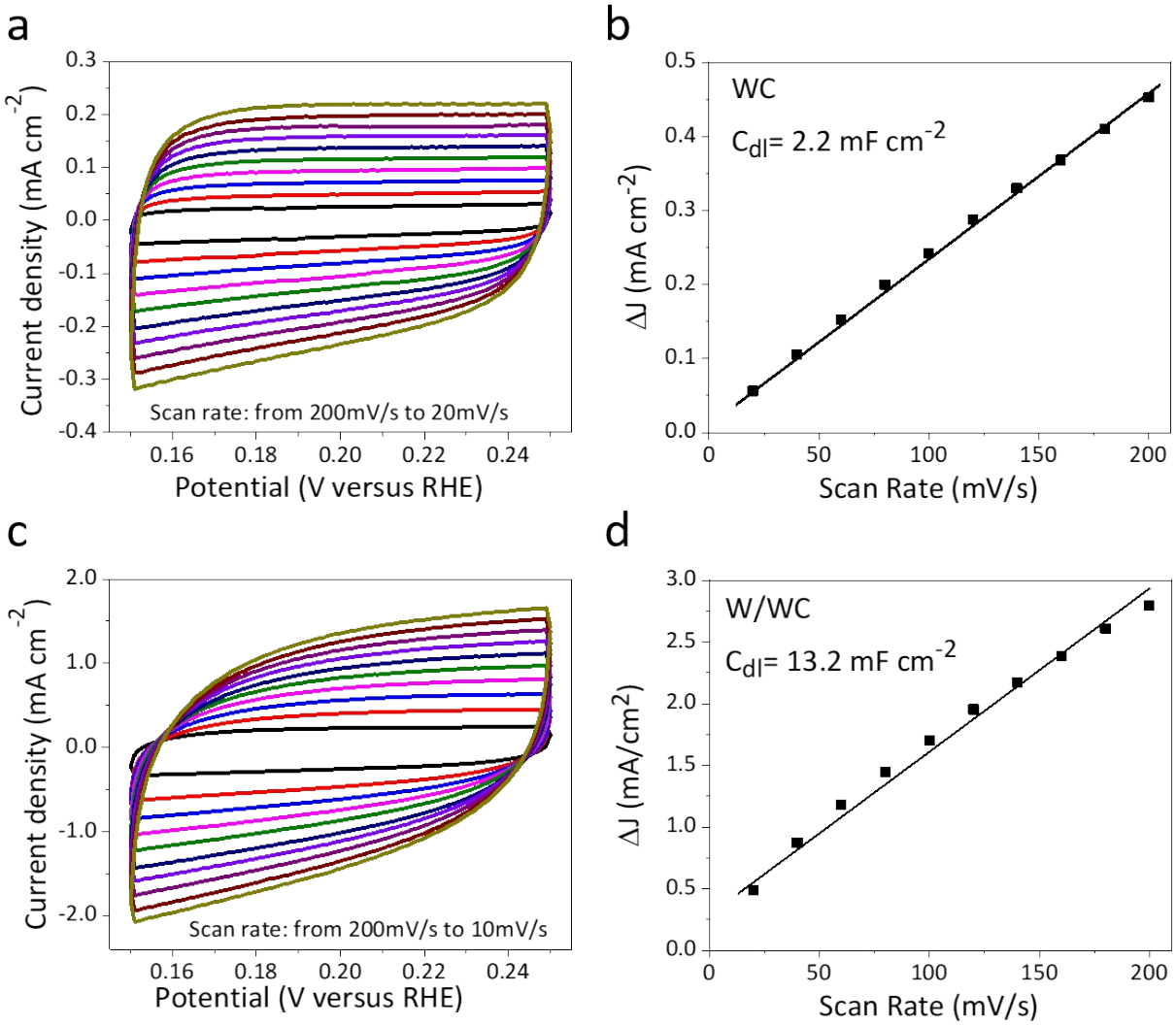

Figure S17. (a, c) CVs with different rates from 20 to 200 mV s^{-1} and (b, d) the capacitive current at 0.2 V as a function of scan rate for (a, b) pristine WC and (c, d) the new produced W/WC heterostructures. The electrochemical double-layer capacitance (EDLC, C_{dll}) was measured to investigate the electrochemically surface area. Cyclic voltammetry (CV) was performed in the region from 0.15 to 0.25 V vs RHE at rates varying from 20 to 200 mV s^{-1}. The C_{dll} of W/WC (13.2 mF cm^{-2}) was six times larger than that of WC precursor (2.2 mF cm^{-2}). Thus, W/WC heterostructures have extremely abundant active sites.

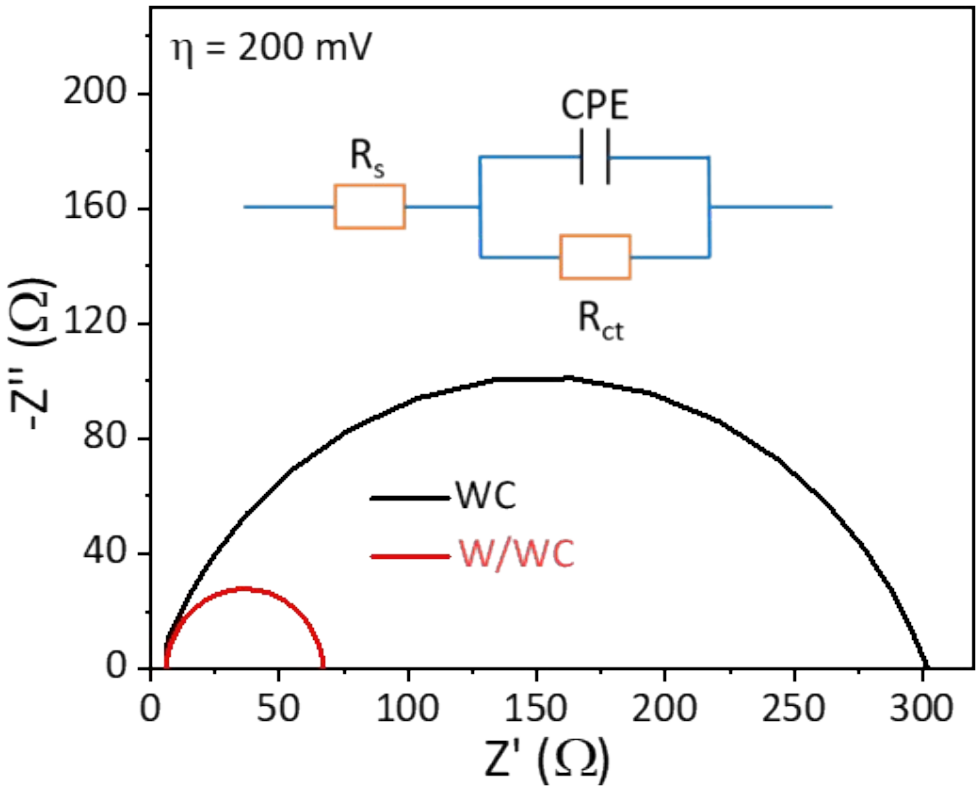

Figure S18. Electrochemical impedance spectrum of W/WC heterostructures and pristine WC at η=200 mV, and the inset image is equivalent circuit diagram.

The interface reactions and electrode kinetics of the catalysts in the HER can be further manifested by electrochemical impedance spectroscopy (EIS) [7]. The Nyquist plots of all the samples and the corresponding electrical equivalent circuit diagram are given in Figure S18, where the ohmic series resistance (Rs) was fitted by the intercept of the semicircle on the real axis, and the charge transfer resistance (R_{ct}) was assigned to the semicircle of the Nyquist plot in terms of the equivalent circuit model. The R_s of the two samples locate in the range of 5.8-6.0 Ω, which indicates the good conductivity of the electrodes. The W/WC heterostructures present the smaller R_{ct} (67 Ω) than that of the WC precursor (301 Ω). It has been well established that the R_{ct} is related to the electrocatalytic kinetics, and a lower R_{ct} value corresponds to a faster reaction rate [5].

S12. Tables 1-3

Table S1. A survey of reaction configurations reported in literature.

Literature	Carbide precursor	Temperature range	X[a]	Compositions
Carbon **2011**, 49, 4427-4433.	WC	700-1100 °C	>10	Graphene-like carbon nanosheets
Carbon **2007**, 45, 2717-2722.	VC	500-1100 °C	28.1	Nanoporous carbon powder
Microporous Mesoporous Mater. **2004**, 72, 203–208.	B_4C	400-1200 °C	10	Graphite ribbons or amorphous carbon
J. Power Sources **2006**, 158, 765-772.	ZrC/TiC	600-1200 °C	10	Multi-layered graphene sheets
Energy Environ. Sci. **2010**, 3, 223-227.	ZrC	800 °C	8.3	Nanoporous carbon powder
Science **2010**, 328, 480-483.	TiC	500 °C	>10	Nanoporous carbon film
ACS Nano **2010**, 4, 1337–1344.	SiC	700-900 °C	>10	Ordered mesoporous carbon nanotubes
Carbon **2009**, 47, 23-29.	Mo_2C	400-1200 °C	4.9	Nanoporous carbon powder
Adv. Funct. Mater. **2013**, 23, 1081-1089.	TiC	2400-1200 °C	10	Few-layered graphitic carbon sheets
This work	WC	950-1050 °C	0-2.6	W/WC or WC@CDC

[a] χ reported in these works are normalized because they used volume of chlorine as benchmark, and we converted the volume into molar value at the normal temperature-pressure (273.15K and 101.325 KPa).

Table S2. The products under various experimental configurations.

Product	Temperature (℃)	χ	Holding time (h)
WC@W/WC	950	1.3	4
W/WC	1000	1.3	4
Broken W/WC	1050	1.3	4
Sinstering WC	1000	0	4
WC@CDC	1000	2.6	4
WC@NLG	1000	1.3	8

Table S3. The comparison of experimental and calculated lattice constants for hexagonal WC.

Lattice parameter	Experimental	Calculated	Difference (%)
a	2.906	2.930	0.8
b	2.906	2.930	0.8
c	2.838	2.832	0.2

Table S4. A survey of the PEC performances of Si nanowire based photocathodes from literatures.

Reference	Photocathode	Electrolyte	Photocurrent density @ 0 V (mA cm^{-2})
This work	p-Si NWs@W/WC	0.5 M H_2SO_4	16
Nat. Commun. 2016, **7**, 13216.	p-Si NWs@W_2C	0.5 M H_2SO_4	16
J. Am. Chem. Soc. 2015, **137**, 7035.	a-Si@Mo_2C	1 M KOH	11.5
Langmuir 2016, **32**, 11728.	H-Si@Pt NPs	0.5 M H_2SO_4	15.5
ACS Appl. Mater. Interfaces 2018, **10**, 17280.	p-Si NWs@$WS_{2-x}P_x$	0.5 M H_2SO_4	19.1
Nano Energy 2017, **32**, 422.	p-Si NWs@$CoMoS_x$	0.5 M H_2SO_4	17.2
ACS Energy Lett. 2017, **2**, 1939.	p-Si NWs@NiFeLDH	0.5 M H_2SO_4	7

S13. References

[1] Blöchl, P. Projector augmented-wave method. *Phys. Rev. B* **1994**, *50*, 17953.

[2] Kresse, G., Joubert, D. From ultrasoft pseudopotentials to the projector augmented-wave method. *Phys. Rev. B* **1999**, *59*, 1758.

[3] Paier, J., Hirschl, R., Marsman, M., Kresse, G. The Perdew–Burke–Ernzerhof exchange-correlation functional applied to the G2-1 test set using a plane-wave basis set. *J. Chem. Phys.* **2005**, *122*, 234102.

[4] Liu, H., Neal, A., Zhu, Z., Xu, X., Tomanek, D., Ye, P., Luo, Z. Phosphorene: an unexplored 2D semiconductor with a high hole mobility. *ACS nano* **2014**, *8*, 4033-4041.

[5] Nørskov, J., Bligaard, T., Logadottir, A., Kitchin, J., Chen, J., Pandelov, S., Stimming, U. Trends in the exchange current for hydrogen evolution. *J. Electrochem. Soc.* **2005**, *152*, J23-J26.

[6] Gong, Q., Wang, Y., Hu, Q., Zhou, J., Feng, R., Duchesne, P. N., Zhang, P., Chen, F., Han, N., Li, Y., Jin, C., Li, Y., Lee, S. T., Jin, C. Ultrasmall and phase-pure W_2C nanoparticles for efficient electrocatalytic and photoelectrochemical hydrogen evolution. *Nat. Commun.* **2016**, *7*, 13216.

[7] Xing, Z., Liu, Q., Asiri, A., Sun, X. Closely Interconnected Network of Molybdenum Phosphide Nanoparticles: A Highly Efficient Electrocatalyst for Generating Hydrogen from Water. *Adv. Mater* **2014**, *26*, 5702.